Nonsymmetric formation of Δ^1-piperideine from lysine in plants via a bacterial-like PLP-dependent enzyme

Catharine X. Wood[1,2], Oriana Serna Daza[1], Katherine Newling[3], Sally James[3], William P. Unsworth[2] and Benjamin R. Lichman[1]*

[1]Centre for Novel Agricultural Products, Department of Biology, University of York, York, YO10 5DD UK

[2]Department of Chemistry, University of York, York, YO10 5DD UK

[3]Biosciences Technology Facility, Department of Biology, University of York, York, UK.

*Correspondence to: benjamin.lichman@york.ac.uk

Abstract

Piperidine alkaloids in plants derive from lysine via Δ^1-piperideine. We investigated the alkaloid biosynthesis in *Flueggea suffruticosa*, a plant that produces diverse piperidine alkaloids, including securinine. Until now, pathways leading to the formation of Δ^1-piperideine have involved two enzymatic steps: a decarboxylase and an oxidase, proceeding via free cadaverine. We discovered Δ^1-piperideine synthase (PS), a PLP-dependent enzyme that forms Δ^1-piperideine directly from lysine via an oxidative deamination. We demonstrate that PS catalyses this transformation in a non-symmetric manner, and show it is positioned within the group III decarboxylase family, which is typically associated with prokaryotes. We also identified a paralog gene exhibiting decarboxylase activity. This work delineates the first enzymatic step in the biosynthesis of securinine as an unprecedented oxidative deamination of lysine. It also marks the identification of the first eukaryotic group III decarboxylase and resolves the longstanding question of non-symmetric nitrogen incorporation in piperidine alkaloids.

Introduction

Alkaloids, naturally occurring nitrogen-containing compounds, are highly diverse in the plant kingdom[1]. As specialised metabolites, they are taxonomically restricted and provide an ecologically adaptive role such as defence against pathogens and herbivores[2]. Alkaloids or their derivatives are widely used as pharmaceuticals[3,4]. Several notable plant alkaloids are derived from lysine via $\Delta^{\mathbf{1}}$-piperideine, including huperzine A (*Lycopodium*)[5,6] and lupinine (*Lupinus*)[7,8] (**Fig. 1A**). The biosynthesis of these piperidine alkaloids has been under intensive investigation, with the aim of discovering the pathway enzymes to allow either formation of alkaloids in heterologous systems[9,10] or the elimination of alkaloid biosynthesis in host tissues[7,11].

The alkaloid securinine[12], found in *Flueggea suffruticosa* and related species, is a highly bioactive GABA-receptor antagonist[13] and also derived from lysine via $\Delta^{\mathbf{1}}$-piperideine (**Fig. 1B**)[14]. It is a representative of the *Securinega* alkaloids, a family of polycyclic compounds with stereochemical and skeletal diversity (**Fig. 1C**)[15]. The structures and bioactivities of these compounds has led to interest in their formation, and consequently they have been the subject of many recent total synthesis campaigns[16–18]. However, only one enzyme involved in the biosynthesis of *Securinega* alkaloids has been described, an oxidase acting on allosecurinine[19]. No enzymes acting in the formation of securinine have been reported.

The biosynthetic formation of $\Delta^{\mathbf{1}}$-piperideine from lysine has been described in the *Lycopodium*[20,21] and lupin[22,23] alkaloid pathways and involves two enzymes: lysine decarboxylase (LDC) catalysing the formation of cadaverine from lysine, and then a copper amine oxidase (CAO) catalysing oxidation of cadaverine into 5-aminopentanal, which spontaneously cyclises into $\Delta^{\mathbf{1}}$-piperideine (**Fig. 1D**). Plants do not typically have a dedicated LDC, and these alkaloid enzymes appear to have evolved on

multiple occasions from ornithine decarboxylases (ODCs) which are part of the group IV decarboxylase family[20].

Isotope labelling experiments have shown that lysine can be incorporated into alkaloids either through a symmetric or nonsymmetric manner (**Fig. 1D**)[24]. The symmetrical pathway implies an intermediate with a plan of symmetry (i.e. cadaverine), whereas the non-symmetrical pathway no symmetrical intermediate is present. It has been proposed that a PLP-bound cadaverine could act as the non-symmetrical intermediate in the non-symmetric pathway[24]. *Lycopodium*[25] and lupin[26] alkaloid labelling shows a symmetric pathway, in line with the two enzymes discovered and the intermediacy of cadaverine. In contrast, the securinine[14] and anabasine[27] pathways have been found to proceed via a non-symmetric pathway. No non-symmetric enzymatic pathway to Δ^{1}-piperideine has been characterised.

We aimed to discover the first steps of securinine alkaloid biosynthesis, with a long-term ambition to elucidate the biosynthetic pathway of this natural product and related *Securinega* alkaloids. We first set out to identify an LDC from *F. suffruticosa*, but in doing so we discovered a single enzyme capable of catalysing the formation of Δ^{1}-piperideine from lysine: Δ^{1}-piperideine synthase (PS) (**Fig. 1D**). We then showed the enzyme generates H_2O_2, indicating oxidative activity, and used isotope labelling to demonstrate nonsymmetric incorporation of lysine into Δ^{1}-piperideine. Sequence homology shows PS is a member of the group III decarboxylase family, which is typically associated with prokaryotes and features no characterised eukaryotic sequences prior to this work. We also identified a PS paralog (PSP) with lysine and arginine decarboxylase activities. This work opens the door to further examination of securinine alkaloid biosynthesis but also has implications for polyamine and alkaloid biosynthesis in plants more broadly.

Results

Identification of lysine decarboxylase candidates

The first step towards elucidation of piperidine alkaloid biosynthesis in *F. suffruticosa* was the formation of a transcriptomic resource. We isolated and sequenced RNA from 15 samples of different tissues and developmental stages of *F. suffruticosa* (**Table S1**). We combined short read Illumina and long-read Nanopore sequencing to assemble a *de novo* transcriptome, and then aligned the short-read sequences to obtain gene expression levels across the samples (**Fig. S1**).

We set out to discover a lysine decarboxylase that we expected to catalyse the first step in the formation of Δ^{1}-piperideine that contributes the securinine piperidine ring. We identified five gene candidates in the transcriptome via InterProScan functional annotations matching ornithine or arginine decarboxylase (genes 25968, 4074, 4984, 3498 and 1864; **Table S2**)[28]. Assessment of the gene sequences revealed that the coding sequence in gene 25968 was a truncated isoform of gene 4074, and so the

gene was removed from the list (**Fig. S2**). Gene 3498 was also excluded from further assessment due to low gene expression across all samples (**Fig. S3**). This left three candidates to examine for LDC activity.

Lysine decarboxylase screening

To obtain enzyme for assays, we initially attempted to heterologously express and purify full length LDC candidates in *E. coli*. However, after numerous unsuccessful attempts we switched to the *Nicotiana benthamiana* transient expression system, a robust platform for screening plant enzymes[9]. Rather than rely on endogenous pools of lysine, we instead used leaf disc experiments where, five-days post-infiltration, leaf discs containing heterologously expressed enzymes are excised and incubated with lysine.

By employing this method, we were able to observe consumption of lysine and accumulation of cadaverine in the positive control, *Lupinus angustifolius* LDC (**Fig. 2**)[22]. We saw limited accumulation of cadaverine in leaf discs expressing gene 3498. For gene 1864, we saw consumption of lysine, but no accumulation of cadaverine. Instead, we saw accumulation of a peak matching the retention time and mass of a synthesised Δ^1-piperideine standard (**Fig. 2**). It appeared that gene 1864 encoded an enzyme able to convert lysine directly to Δ^1-piperideine.

$\Delta^{\mathbf{1}}$-Piperideine is not stable as it is prone to spontaneous isomerisation, dimerisation, trimerisation and higher oligomerisation, equilibrating in solution, with the dominant form in solution being dependent on the solvent and pH[29]. This behaviour may contribute to its biosynthetic role in some alkaloid pathways, such as that recently described in lupin alkaloid biosynthesis[11]. However, these properties can make analysis challenging, hence why we detect it at the dimer mass ($[2M+H]^+$ = 167), and why the peak shape is not typically Gaussian.

$\Delta^{\mathbf{1}}$-Piperideine synthase

To verify the unusual activity of the enzyme encoded by gene 1864, we returned to *E. coli* recombinant expression. AlphaFold structural model analysis revealed that the enzyme contained a highly unstructured extended N-terminus (**Fig. 3A**). Consequently, we truncated the N-terminal by 74 amino acids and obtained the gene with codon optimisation and an N-terminal His-tag. With this new construct, we were able to obtain the recombinant gene 1864 enzyme product with sufficient concentration and purity for *in vitro* assays (**Fig. S4A**).

Incubation of the purified enzyme with lysine and PLP led to the formation of Δ^1-piperideine (**Fig. 3B**), validating the leaf disc assays. Based on these results we have named the enzyme encoded by gene 1864 as Δ^1-piperideine synthase (PS). We propose the enzyme catalyses decarboxylation followed by oxidation and deamination to form the aldehyde 5-aminopentanal. The cyclisation of this aldehyde into Δ^1-

piperideine is favoured in water. To our knowledge this is the first report of an enzyme catalysing the formation of Δ^1-piperideine directly from lysine.

Despite this novelty, there is considerable precedence for PLP-dependent enzymes catalysing decarboxylation - oxidative deamination reactions[30], such as plant amino acid aldehyde synthases[31] and bacterial enzymes catalysing the oxidative deamination of ornithine[32,33]. These enzymes appear to have a common mechanism which involves O_2 as a co-substrate, and CO_2, H_2O_2 and NH_3 as products (**Fig. S5**)[30].

To assess whether PS shares this common mechanism, we coupled the *in vitro* reaction with a peroxidase assay to show that H_2O_2 accumulates over the course of the reaction (**Fig. 3C, Fig. S4B**).

Non-symmetric isotope labelling

Isotope labelling experiments in *F. suffruticosa* had shown that Δ^1-piperideine in securinine originates from lysine in a non-symmetrical manner[14]. With the enzyme responsible for this transformation now in hand, we were able to examine this phenomenon *in vitro*. To achieve this, we obtained ε^{15}N, ε^{13}C-lysine and used it as a substrate for PS.

There are two possible routes to Δ^1-piperideine from lysine (**Fig. 4A**). In the step-wise route, where the reaction occurs via a free cadaverine intermediate, we would expect to have a scrambled, symmetric signal and to observe both singly and doubled labelled products, which would provide a mixture of three dimer masses, $[2M+H]^+$ = 169, 170 and 171. In a concerted route, where the decarboxylated intermediate is enzyme bound, we would observe only the double labelled product: $[2M+H]^+$ = 171. When PS was supplied with ε^{15}N, ε^{13}C-lysine, only the doubly labelled product was observed, indicating a concerted reaction (**Fig. 4B**).

To determine the position of the isotope labels on the product, we analysed the enzyme product using ^{13}C-NMR (**Fig. 4C**). The spectra were obtained directly from enzyme assays conducted in water; hence the product is present as a mixture of forms. With ε^{15}N, ε^{13}C-lysine as the substrate, we observe 13C peaks at 30-70 ppm, consistent with sp^3-hybridised carbon atoms adjacent to a heteroatom. As a control, we wanted to compare the peaks to the full ^{13}C-spectrum of the enzyme product in water. To do this, we obtained the fully ^{13}C-labelled $^{13}C_6$-lysine and used it as an enzyme substrate. In the product, we noted the presence of sp^2 hybridised (likely imine/iminium signals) and aldehyde peaks, which may be derived from the lysine αC or εC if the reaction occurred via a free cadaverine, but only the αC in a concerted reaction. These peaks are absent in the ε^{15}N, ε^{13}C-lysine derived reaction, suggesting the equivalent sp^2 and aldehyde peaks are derived from the unlabelled αC and therefore not visible on the spectrum.

This *in vitro* labelling study confirms, via both mass-spectrometry and ^{13}C-NMR, a concerted reaction mechanism without a free intermediate and provides an enzymatic explanation for the nonsymmetric labelling observed in the plant.

Prokaryotic-like decarboxylases

LDCs are not universally found in plants; characterised LDCs operating in plant specialised metabolism have evolved from ODCs on multiple independent occasions[20]. The tendency of plant LDCs to evolve convergently alongside the unprecedented oxidative deamination catalysed by PS prompted an investigation into the enzyme's evolutionary origin.

Based on annotation and sequence similarity PS is a member of the PLP-dependent group III decarboxylase family (InterPro: major domain, IPR000310; family IPR011193)[34,35]. This group is part of the larger PLP-dependent fold I superfamily, which also includes group II decarboxylases (InterPro: family IPR002129), which feature plant amino acid decarboxylases and aldehyde synthases[36,37]. Notably this is a different fold type and decarboxylase group to typical plant LDC/ODCs, which are group IV decarboxylases (InterPro: family IPR000183), with PLP fold type III. Structures of representatives of these sequences including PS confirm the sequence-based relationships (**Fig. 5A**).

The decarboxylase group III is typically known as the prokaryotic-type ornithine/lysine/arginine (Orn/Lys/Arg) decarboxylases. To our knowledge, there is only a single report of eukaryotic enzymes related to this group[38], and no decarboxylase group III eukaryotic enzymes have been characterised. In the InterPro IPR000310 entry, representing the major domain of the group III decarboxylases, there are 26,000 bacterial sequences and less than 1000 from eukaryotes.

We constructed a phylogenetic tree of group III decarboxylases, based on the presence of the major domain (InterPro: IPR000310) and focussing on eukaryotic sequences (**Fig. 5B, Fig. S6**). We used group II decarboxylases as an outgroup and we only included reviewed prokaryotic sequences. Ignoring single reports from a clade, which could be the result of contamination, the phylogenetic tree reveals at least four origins of group II decarboxylases in eukaryotes. There appear to be gammaproteobacteria arginine decarboxylase (ADC) like genes in Amoebozoa. There is also a eukaryotic lineage sister to gammaproteobacterial Orn/Lys/Arg decarboxylases found in flatworms and Apicomplexa protists. Bacillus-like ADCs appear in rotifers, microscopic animals.

The eukaryotic group III decarboxylase lineage leading to PS has an algal origin, found in red, green and ochrophyte algae. It is also widespread in green plants: there are orthologs in bryophytes, monocots (including rice, maize and wheat), asterids and rosids. However, no homologs were identified in gymnosperms, nor in Arabidopsis.

Examination into the origin of PS appears to have revealed a hitherto neglected family of plant enzymes, which may have wider roles in polyamine biosynthesis.

Piperideine synthase paralog

To examine PS evolution more closely, we inferred a phylogenetic tree of homologs from the rosid clade of flowering plants (**Fig. 5C**). This analysis revealed the presence of a homolog of PS also present in *F. suffruticosa.* This paralog is gene 3498, which was previously excluded from screening due to low expression. PS and this PS-paralog (PSP) are sister sequences yet share only 54% sequence identity. Furthermore, PS has <60% sequence identity with orthologs from Malpighiales, whereas PSP has >65% identity with the same sequences. Altogether this indicates a gene duplication and activity divergence event in the *Flueggea* lineage, where PSP maintained ancestral-like activity and PS evolved new activity related to alkaloid biosynthesis.

Based on this hypothesis, we elected to test the activity of PSP, to further interrogate the activities of plant group III decarboxylases and the evolution of PS. We expressed a N-terminally truncated form of the enzyme in *E. coli*. The activity tests with lysine revealed limited piperideine synthase activity compared to PS, but instead demonstrate decarboxylase activity, forming cadaverine (**Fig. 5D**). The enzyme was also shown to decarboxylate arginine into agmatine, which PS is not capable of doing (**Fig. 5E**).

An alignment of PS and PSP with PLP fold I decarboxylases highlights the conserved lysine residue responsible for PLP binding (**Fig. S7**). The tyrosine residue involved in protonation of the PLP intermediate in decarboxylases (**Fig. S5**) is present in PSP but absent from PS, where it is substituted with an asparagine (**Fig. S7A**). The substitution of the equivalent tyrosine residue has been observed in the evolution of amino acid aldehyde synthases (AAASs) from type II decarboxylases, where they are typically substituted for a phenylalanine[31].

We performed mutations to swap the asparagine in PS with the tyrosine from PSP, and vice versa, and analysed the activity of the recombinantly produced enzymes by LC-MS (**Fig. 5D**). With lysine as the substrate, PS-N265Y shows reduced levels of Δ^1-piperideine formation compared to PS but no notable increase in cadaverine formation. The Y264N substitution eliminates lysine decarboxylase activity in PSP but does not increase Δ^1-piperideine formation compared to the wild-type PSP. The tyrosine therefore appears necessary but not sufficient for cadaverine formation. Further residues are likely to be involved in oxidase activities.

Discussion

Plant alkaloids are amino acid derived and often feature complex polycyclic structures and biological activities[1]. They can be classified by the source of their nitrogen and the

type of ring it is found in. However, these classes are not necessarily evolutionarily related and have emerged convergently[39]. The LDCs found in piperidine alkaloid biosynthesis are an example of this, with legume LDC and lycopodium LDC emerging from ODCs independently[20]. We set out to discover an LDC involved in *F. suffruticosa* securinine alkaloid biosynthesis with an expectation that we would discover an LDC with another convergent origin.

Rather than identifying this hypothesised LDC, we instead discovered a PLP-dependent enzyme capable of converting lysine directly to Δ^1-piperideine, an enzyme catalysed conversion not previously described. This enzyme catalyses both decarboxylation and subsequent oxidation of lysine, meaning that a single enzyme is required for the formation of Δ^1-piperideine whereas typically two are used, an LDC and CAO. Therefore, Δ^1-piperideine biosynthesis in *F. suffruticosa* is indeed of convergent origin but not via a typical plant LDC.

Early investigations into piperidine alkaloid biosynthesis in plants employed isotope labelling and identified two types of pathways: pathways with symmetric incorporation of the lysine "C_5N" unit (e.g. *Lycopodium* and lupin alkaloids) and those with nonsymmetric "C_5N" incorporation (e.g. securinine, anabasine). The symmetric pathway goes via a free cadaverine. Using isotope labelling in the *in vitro* reaction we have demonstrated an enzymatic explanation for a nonsymmetric route, via a bound cadaverine-PLP intermediate, as predicted by Leistner and Spenser[24].

Oxidative deamination reactions catalysed by PLP-dependent enzymes are well known for substrates beyond lysine[30]. Bacterial ODCs have been shown to convert ornithine into Δ^1-pyrroline, CO_2, NH_3 and H_2O_2, using O_2 as a co-substrate[32,40]. In an evolution experiment in *E. coli* the ODC SpeC underwent mutations converting it into an oxidative deaminase[33]. Plant aromatic amino acid aldehyde synthases (AAASs) catalyse the same oxidative deamination and have emerged repeatedly from aromatic amino acid decarboxylases (AAADs) and feature in multiple biosynthetic pathways[31].

The evolutionary origin of PS is particularly surprising, emerging, not like typical plant LDCs from group IV decarboxylases (PLP-fold type III) but instead from group III decarboxylases (PLP-fold type I). PS and its paralog PSP are the first characterised eukaryotic sequences from this family, previously thought to be limited to bacteria. The phylogenetic analysis suggests that PSP is the more typical member of this family, with PS arising through duplication and divergence. The general role of the plant group III decarboxylases in the plant lineage is unknown, but as PSP was shown to decarboxylate lysine and arginine, it is possible these are involved in polyamine biosynthesis as part of primary metabolism[41].

PS is the first enzyme discovered in the pathway to securinine. It has a crucial role in the origin of the nitrogen and in the transition between primary and specialised metabolism. The PS gene can therefore be used as a bait to find other securinine alkaloid pathway genes via transcriptomic and genomic methods[42] for plant pathway

discovery. In attempting to elucidate securinine alkaloid biosynthesis we have revealed enzyme types with potential implications across alkaloid pathways and perhaps primary plant metabolism.

Data availability

Raw read sequences for all generated data in this study are available in the National Center for Biotechnology Information Sequence Read Archive under BioProject ID PRJNA1106657. Sequences of coding sequences of genes are available on GenBank: gene 1864 (PS) (PP748646), gene 3498 (PSP) (PP748647), gene 4984 (PP748648) and gene 4074 (PP748649). All other data is available upon reasonable request to the corresponding author.

References

1. Lichman, B. R. The scaffold-forming steps of plant alkaloid biosynthesis. *Nat. Prod. Rep.* **38**, 103–129 (2021).
2. Wink, M. Chemical Ecology of Alkaloids. in *Alkaloids: Biochemistry, Ecology, and Medicinal Applications* (eds. Roberts, M. F. & Wink, M.) 265–300 (Springer US, Boston, MA, 1998).
3. Heinrich, M., Mah, J. & Amirkia, V. Alkaloids Used as Medicines: Structural Phytochemistry Meets Biodiversity-An Update and Forward Look. *Molecules* **26**, (2021).
4. Schmeller, T. & Wink, M. Utilization of Alkaloids in Modern Medicine. in *Alkaloids: Biochemistry, Ecology, and Medicinal Applications* (eds. Roberts, M. F. & Wink, M.) 435–459 (Springer US, Boston, MA, 1998).
5. Nett, R. S., Dho, Y., Low, Y.-Y. & Sattely, E. S. A metabolic regulon reveals early and late acting enzymes in neuroactive Lycopodium alkaloid biosynthesis. *Proc. Natl. Acad. Sci. U. S. A.* **118**, (2021).
6. Nett, R. S. *et al.* Plant carbonic anhydrase-like enzymes in neuroactive alkaloid biosynthesis. *Nature* **624**, 182–191 (2023).
7. Frick, K. M., Kamphuis, L. G., Siddique, K. H. M., Singh, K. B. & Foley, R. C. Quinolizidine Alkaloid Biosynthesis in Lupins and Prospects for Grain Quality Improvement. *Front. Plant Sci.* **8**, 87 (2017).
8. Mancinotti, D., Frick, K. M. & Geu-Flores, F. Biosynthesis of quinolizidine alkaloids in lupins: mechanistic considerations and prospects for pathway elucidation. *Nat. Prod. Rep.* **39**, 1423–1437 (2022).
9. Eljounaidi, K. & Lichman, B. R. Nature's Chemists: The Discovery and Engineering of Phytochemical Biosynthesis. *Front Chem* **8**, 596479 (2020).
10. Trenchard, I. J. & Smolke, C. D. Engineering strategies for the fermentative production of plant alkaloids in yeast. *Metab. Eng.* **30**, 96–104 (2015).
11. Mancinotti, D. *et al.* The causal mutation leading to sweetness in modern white lupin cultivars. *Sci Adv* **9**, eadg8866 (2023).
12. Saito, S. *et al.* Structure of securinine. *Tetrahedron* **19**, 2085–2099 (1963).

13. Beutler, J. A. *et al.* Securinine alkaloids: a new class of GABA receptor antagonist. *Brain Res.* **330**, 135–140 (1985).
14. Marek Golebiewski, W., Horsewood, P. & Spenser, I. D. Biosynthesis of securinine: the mode of incorporation of lysine. *J. Chem. Soc. Chem. Commun.* 217–218 (1976).
15. Chirkin, E., Atkatlian, W. & Porée, F.-H. The Securinega alkaloids. *Alkaloids Chem. Biol.* **74**, 1–120 (2015).
16. Antien, K. *et al.* Bio-inspired Total Synthesis of Twelve Securinega Alkaloids: Structural Reassignments of (+)-Virosine B and (-)-Episecurinol A. *Chemistry* **25**, 11574–11580 (2019).
17. Jeon, S., Lee, J., Park, S. & Han, S. Total synthesis of dimeric Securinega alkaloids (-)-flueggenines D and I. *Chem. Sci.* **11**, 10934–10938 (2020).
18. Kang, G., Park, S. & Han, S. Synthesis of High-Order and High-Oxidation State Securinega Alkaloids. *Acc. Chem. Res.* **56**, 140–156 (2023).
19. Fan, Z. *et al.* Discovery and Biosynthesis of Ascorbylated Securinega Alkaloids. *ACS Catal.* **11**, 8818–8828 (2021).
20. Bunsupa, S. *et al.* Molecular Evolution and Functional Characterization of a Bifunctional Decarboxylase Involved in Lycopodium Alkaloid Biosynthesis. *Plant Physiol.* **171**, 2432–2444 (2016).
21. Sun, J., Morita, H., Chen, G., Noguchi, H. & Abe, I. Molecular cloning and characterization of copper amine oxidase from Huperzia serrata. *Bioorg. Med. Chem. Lett.* **22**, 5784–5790 (2012).
22. Bunsupa, S. *et al.* Lysine decarboxylase catalyzes the first step of quinolizidine alkaloid biosynthesis and coevolved with alkaloid production in leguminosae. *Plant Cell* **24**, 1202–1216 (2012).
23. Yang, T. *et al.* Transcript profiling of a bitter variety of narrow-leafed lupin to discover alkaloid biosynthetic genes. *J. Exp. Bot.* **68**, 5527–5537 (2017).
24. Leistner, E. & Spenser, I. D. Biosynthesis of the piperidine nucleus. Incorporation of chirally labeled cadaverine-1-3H. *J. Am. Chem. Soc.* **95**, 4715–4725 (1973).
25. Schütte, H. R. *Biosynthese der Alkaloide*. (Deutscher Verlag der Wissenschaften, 1969).
26. Castillo, M., Gupta, R. N., MacLean, D. B. & Spenser, I. D. Biosynthesis of lycopodine from lysine and acetate. The pelletierine hypothesis. *Canadian Journal of Chemistry* **48**, 1893–1903 (1970).
27. Leete, E. Biosynthesis of the nicotiana alkaloids. XIV. The incorporation of delta 1-piperideine-6-14C into the piperidine ring of anabasine. *J. Am. Chem. Soc.* **91**, 1697–1700 (1969).
28. Jones, P. *et al.* InterProScan 5: genome-scale protein function classification. *Bioinformatics* **30**, 1236–1240 (2014).
29. Sato, H., Uchiyama, M., Saito, K. & Yamazaki, M. The Energetic Viability of Δ^1-Piperideine Dimerization in Lysine-derived Alkaloid Biosynthesis. *Metabolites* **8**, (2018).
30. Hoffarth, E. R., Rothchild, K. W. & Ryan, K. S. Emergence of oxygen- and

pyridoxal phosphate-dependent reactions. *FEBS J.* **287**, 1403–1428 (2020).
31. Torrens-Spence, M. P. *et al.* Structural basis for divergent and convergent evolution of catalytic machineries in plant aromatic amino acid decarboxylase proteins. *Proc. Natl. Acad. Sci. U. S. A.* **117**, 10806–10817 (2020).
32. Sakai, K. *et al.* L-ornithine decarboxylase from Hafnia alvei has a novel L-ornithine oxidase activity. *J. Biochem.* **122**, 961–968 (1997).
33. Pontrelli, S. *et al.* Metabolic repair through emergence of new pathways in Escherichia coli. *Nat. Chem. Biol.* **14**, 1005–1009 (2018).
34. Sandmeier, E., Hale, T. I. & Christen, P. Multiple evolutionary origin of pyridoxal-5'-phosphate-dependent amino acid decarboxylases. *Eur. J. Biochem.* **221**, 997–1002 (1994).
35. Blum, M. *et al.* The InterPro protein families and domains database: 20 years on. *Nucleic Acids Res.* **49**, D344–D354 (2021).
36. Grishin, N. V., Phillips, M. A. & Goldsmith, E. J. Modeling of the spatial structure of eukaryotic ornithine decarboxylases. *Protein Sci.* **4**, 1291–1304 (1995).
37. Liang, J., Han, Q., Tan, Y., Ding, H. & Li, J. Current Advances on Structure-Function Relationships of Pyridoxal 5'-Phosphate-Dependent Enzymes. *Front Mol Biosci* **6**, 4 (2019).
38. Li, B., Liang, J., Hanfrey, C. C., Phillips, M. A. & Michael, A. J. Discovery of ancestral L-ornithine and L-lysine decarboxylases reveals parallel, pseudoconvergent evolution of polyamine biosynthesis. *J. Biol. Chem.* **297**, 101219 (2021).
39. Negin, B. & Jander, G. Convergent and divergent evolution of plant chemical defenses. *Curr. Opin. Plant Biol.* **73**, 102368 (2023).
40. Bertoldi, M., Carbone, V. & Borri Voltattorni, C. Ornithine and glutamate decarboxylases catalyse an oxidative deamination of their alpha-methyl substrates. *Biochem. J* **342 Pt 3**, 509–512 (1999).
41. Chen, D., Shao, Q., Yin, L., Younis, A. & Zheng, B. Polyamine Function in Plants: Metabolism, Regulation on Development, and Roles in Abiotic Stress Responses. *Front. Plant Sci.* **9**, 1945 (2018).
42. Dugé de Bernonville, T., Papon, N., Clastre, M., O'Connor, S. E. & Courdavault, V. Identifying Missing Biosynthesis Enzymes of Plant Natural Products. *Trends Pharmacol. Sci.* **41**, 142–146 (2020).
43. Letunic, I. & Bork, P. Interactive Tree Of Life (iTOL) v5: an online tool for phylogenetic tree display and annotation. *Nucleic Acids Res.* **49**, W293–W296 (2021).
44. Meisel, L. *et al.* A rapid and efficient method for purifying high quality total RNA from peaches (Prunus persica) for functional genomics analyses. *Biol. Res.* **38**, 83–88 (2005).
45. Leger, A. & Leonardi, T. pycoQC, interactive quality control for Oxford Nanopore Sequencing. *J. Open Source Softw.* **4**, 1236 (2019).
46. Martin, M. Cutadapt removes adapter sequences from high-throughput sequencing reads. *EMBnet.journal* **17**, 10–12 (2011).
47. de la Rubia, I. *et al.* RATTLE: reference-free reconstruction and quantification of

transcriptomes from Nanopore sequencing. *Genome Biol.* **23**, 153 (2022).
48. Bray, N. L., Pimentel, H., Melsted, P. & Pachter, L. Near-optimal probabilistic RNA-seq quantification. *Nat. Biotechnol.* **34**, 525–527 (2016).
49. Peyret, H., Brown, J. K. M. & Lomonossoff, G. P. Improving plant transient expression through the rational design of synthetic 5’ and 3’ untranslated regions. *Plant Methods* **15**, 108 (2019).
50. Barker, G. *et al.* Enantioselective, palladium-catalyzed α-arylation of N-Boc pyrrolidine: in situ react IR spectroscopic monitoring, scope, and synthetic applications. *J. Org. Chem.* **76**, 5936–5953 (2011).
51. Mirdita, M. *et al.* ColabFold: making protein folding accessible to all. *Nat. Methods* **19**, 679–682 (2022).
52. Katoh, K. & Standley, D. M. MAFFT multiple sequence alignment software version 7: improvements in performance and usability. *Mol. Biol. Evol.* **30**, 772–780 (2013).
53. Trifinopoulos, J., Nguyen, L.-T., von Haeseler, A. & Minh, B. Q. W-IQ-TREE: a fast online phylogenetic tool for maximum likelihood analysis. *Nucleic Acids Res.* **44**, W232-5 (2016).
54. Kalyaanamoorthy, S., Minh, B. Q., Wong, T. K. F., von Haeseler, A. & Jermiin, L. S. ModelFinder: fast model selection for accurate phylogenetic estimates. *Nat. Methods* **14**, 587–589 (2017).
55. Hoang, D. T., Chernomor, O., von Haeseler, A., Minh, B. Q. & Vinh, L. S. UFBoot2: Improving the Ultrafast Bootstrap Approximation. *Mol. Biol. Evol.* **35**, 518–522 (2018).
56. Guindon, S. *et al.* New algorithms and methods to estimate maximum-likelihood phylogenies: assessing the performance of PhyML 3.0. *Syst. Biol.* **59**, 307–321 (2010).

Acknowledgements

We thank Matthew Davy for running samples on the Jeol-700 NMR. We also thank Dr Ed Bergstom for his training and guidance with the LC-MS instrumentation, and the Centre for Excellence in Mass Spectrometry for equipment. The plasmid pHREAC was a gift from George Lomonossoff (Addgene plasmid #134908). We are grateful for computational support from the University of York High-Performance Computing service, Viking, and the Research Computing team. B.R.L. acknowledges support from UKRI (MR/S01862X/1) and BBSRC (BB/Y003586/1).

Contributions

C.X.W. carried out the nucleic acid extraction, transcriptome analysis, cloning, enzyme purification/characterisation and chemical synthesis. O.S.D. performed the peroxidase assays. S.J. prepared sequencing libraries and ran ONT sequencing. K.N. assembled the transcriptome. W.P.U. assisted in the chemical synthesis and interpretation of NMR data. B.R.L. designed and supervised the project and conducted the phylogenetic analyses. C.X.W. and B.R.L. designed the experimental procedures, analysed data, prepared figures, and wrote the manuscript.

Ethics declarations

Competing interests: The authors declare no competing interests.

Main Figures

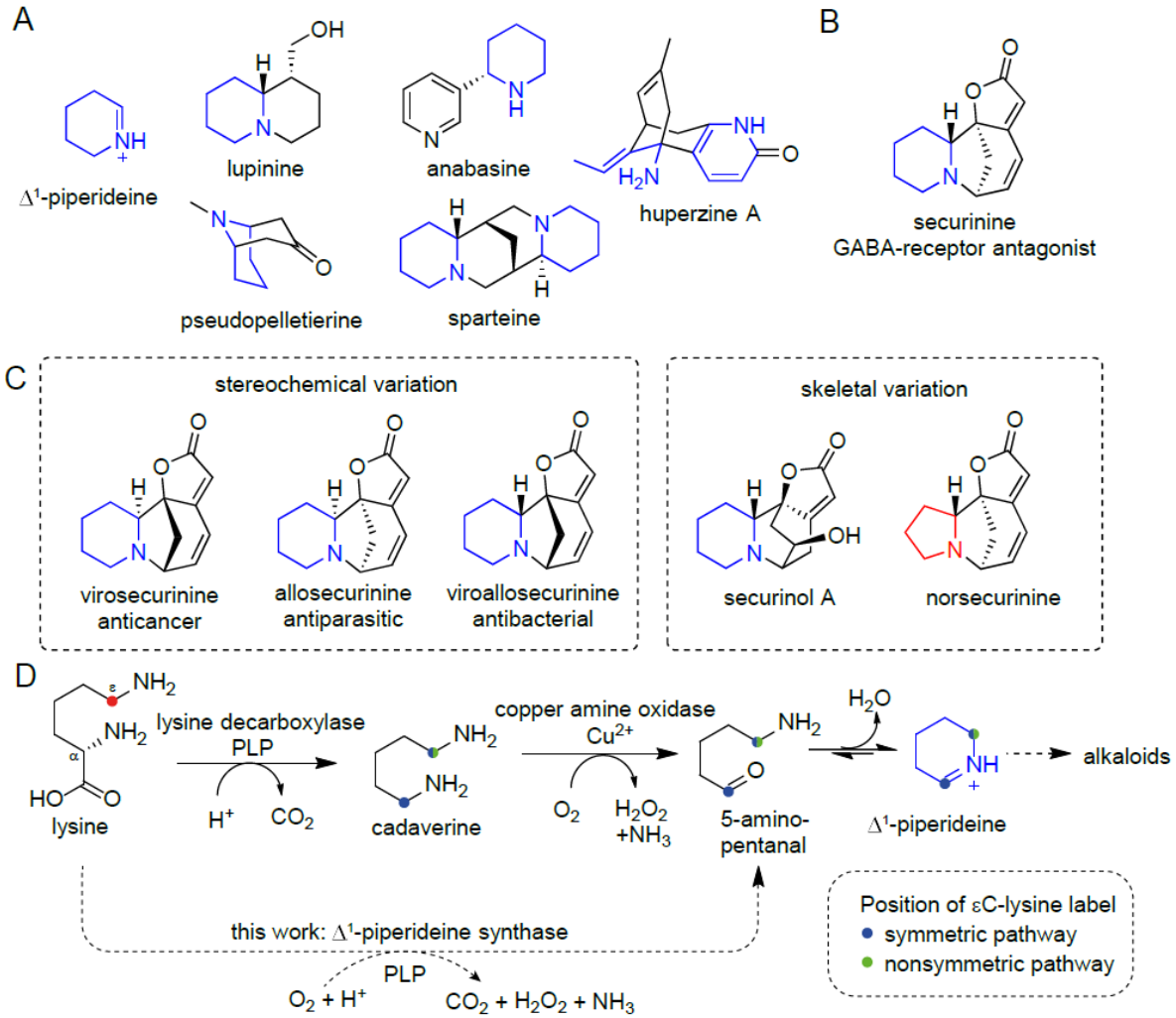

Figure 1. Piperidine alkaloids. A. Structures of Δ^1-piperideine and piperidine alkaloids, with core piperidine moiety in blue. B. Structure of securinine. C. Examples of *Securinega* alkaloids, highlighting stereochemical and skeletal variation, with bioactivities noted. D. Biosynthetic formation of Δ^1-piperideine by the classic two step symmetric pathway or by newly reported nonsymmetric Δ^1-piperideine synthase catalysed route.

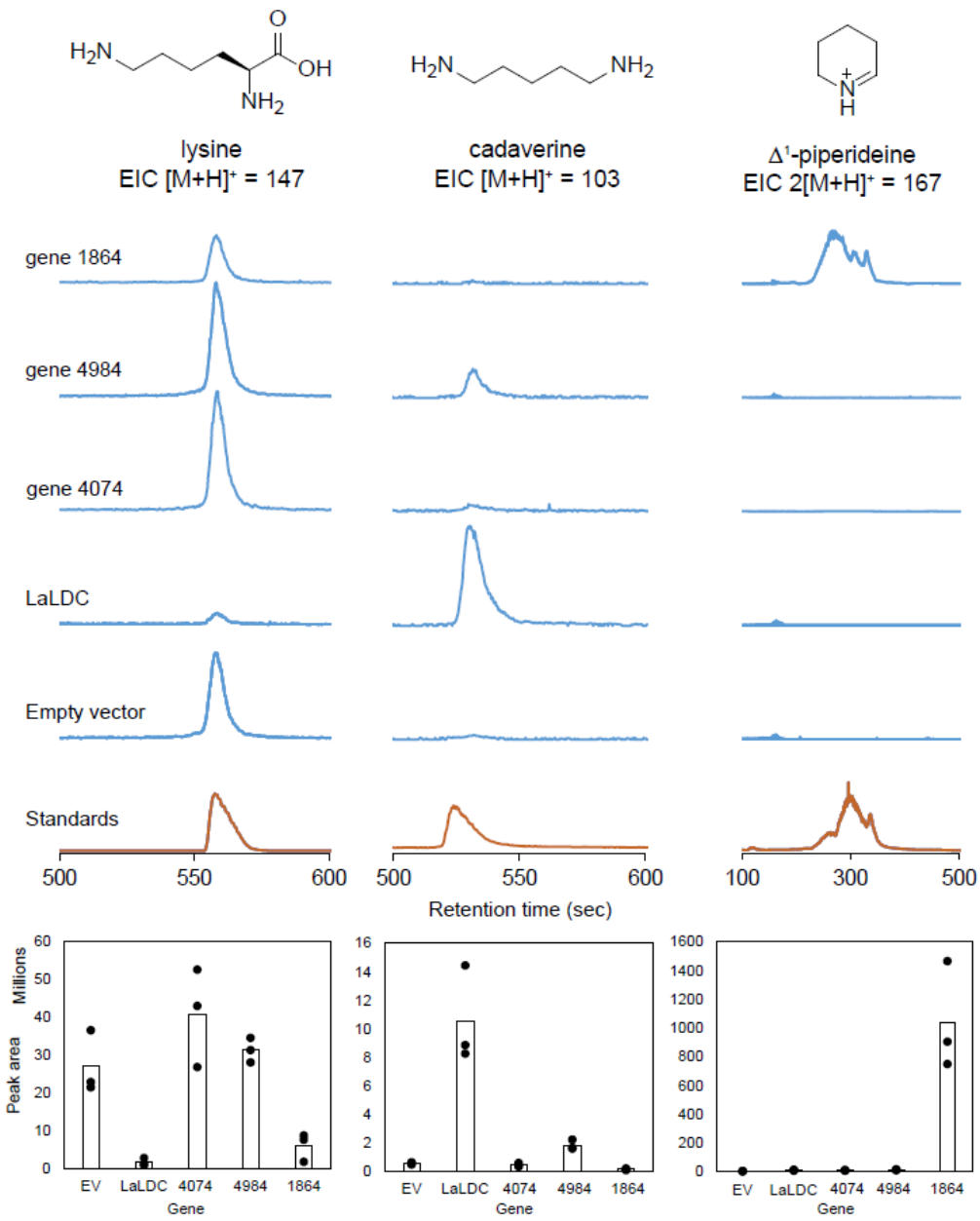

Figure 2. Screening of lysine decarboxylases. LC-MS analysis of leaf disc assays. Different LDC candidate genes were infiltrated into *Nicotiana benthamiana* leaves, then leaf discs were excised and incubated with lysine prior to analysis. Representative chromatograms are extracted ion chromatograms (EIC) for (L-R) lysine, cadaverine and Δ^1-piperideine dimer. Peak height in each EIC is comparable across samples; standards intensities were scaled. Bar graphs underneath show corresponding EIC peak areas; bars show mean of triplicate reactions, points show from each reaction. All areas were blank corrected to the average area of the non-infiltrated plants. *Lupinus angustifolius* LDC (LaLDC) is positive control, empty vector (EV) is negative control.

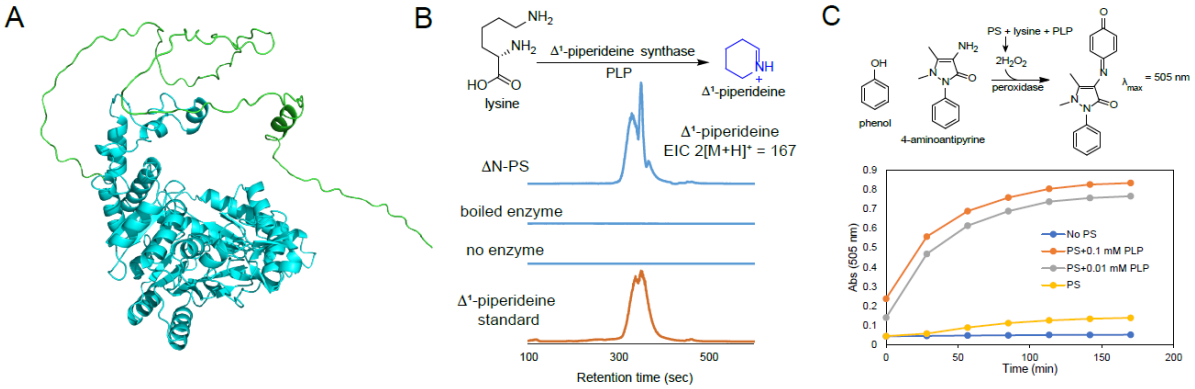

Figure 3. *In vitro* validation of Δ¹-piperidiene synthase activity. A. AlphaFold structural model of Δ¹-piperidiene synthase (PS) monomer with long N-terminus highlighted in bright green and globular fold in aqua. B. *In vitro* assay of recombinant PS showing formation of Δ¹-piperidiene from lysine with additional PLP. C. Coupled enzyme assays showing H_2O_2 production in PS over time. Supplemental PLP aided the reaction.

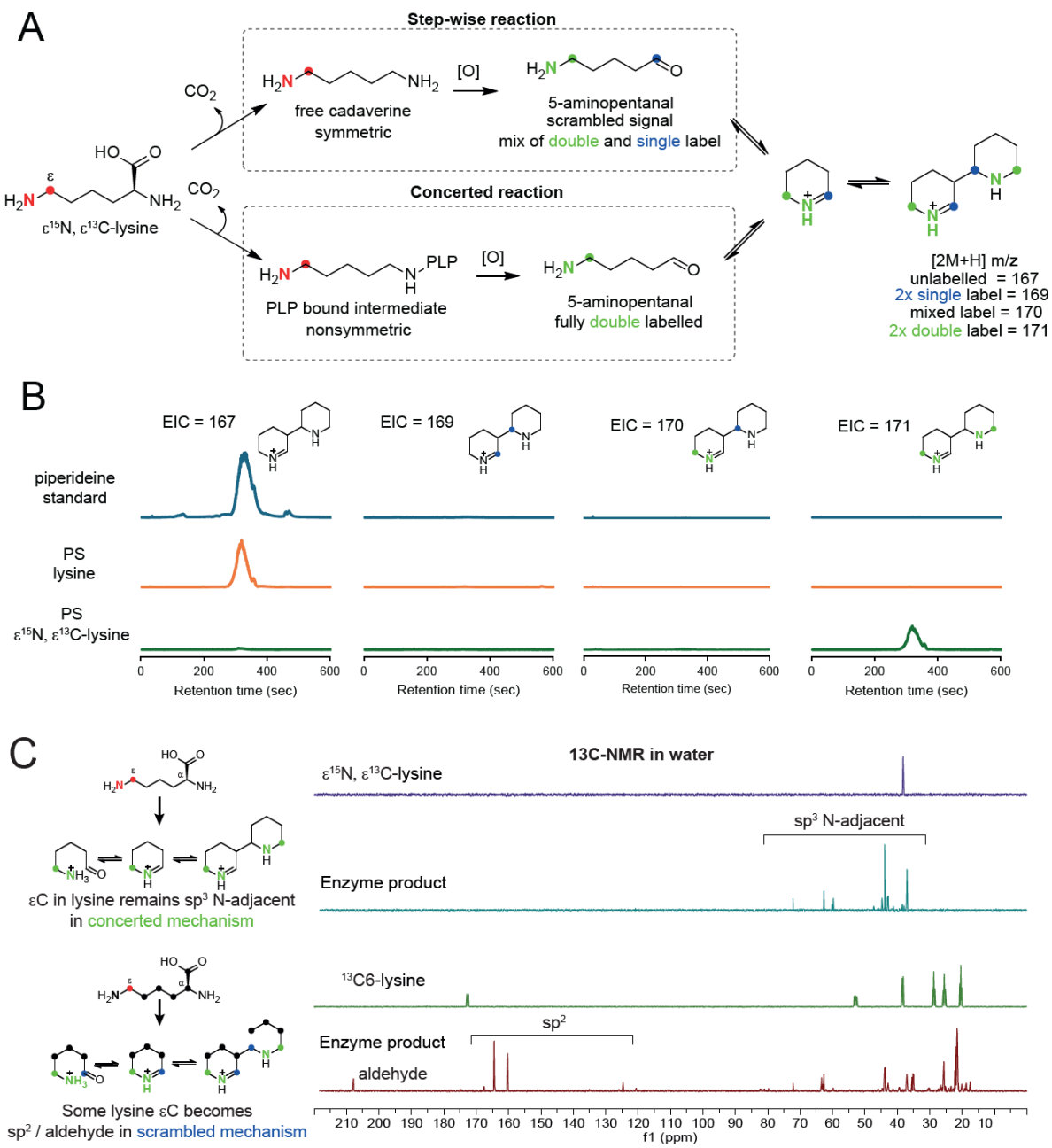

Figure 4. Nonsymmetric formation of Δ¹-piperideine by PS. A. Isotope labelling outcomes of stepwise (i.e. free cadaverine intermediate) or concerted (i.e. bound intermediate) formation of Δ^1-piperideine using ε^{15}N, ε^{13}C-lysine. B. LC-MS results of PS reaction with unlabelled lysine or ε^{15}N, ε^{13}C-lysine. EICs of Δ^1-piperideine dimers: unlabelled (167), 2x single labelled (169), single+double labelled (170) and 2x double labelled (171). C. ^{13}C-NMR of ε^{15}N, ε^{13}C-lysine substrate and PS product compared to fully labelled 13C6-lysine and PS product.

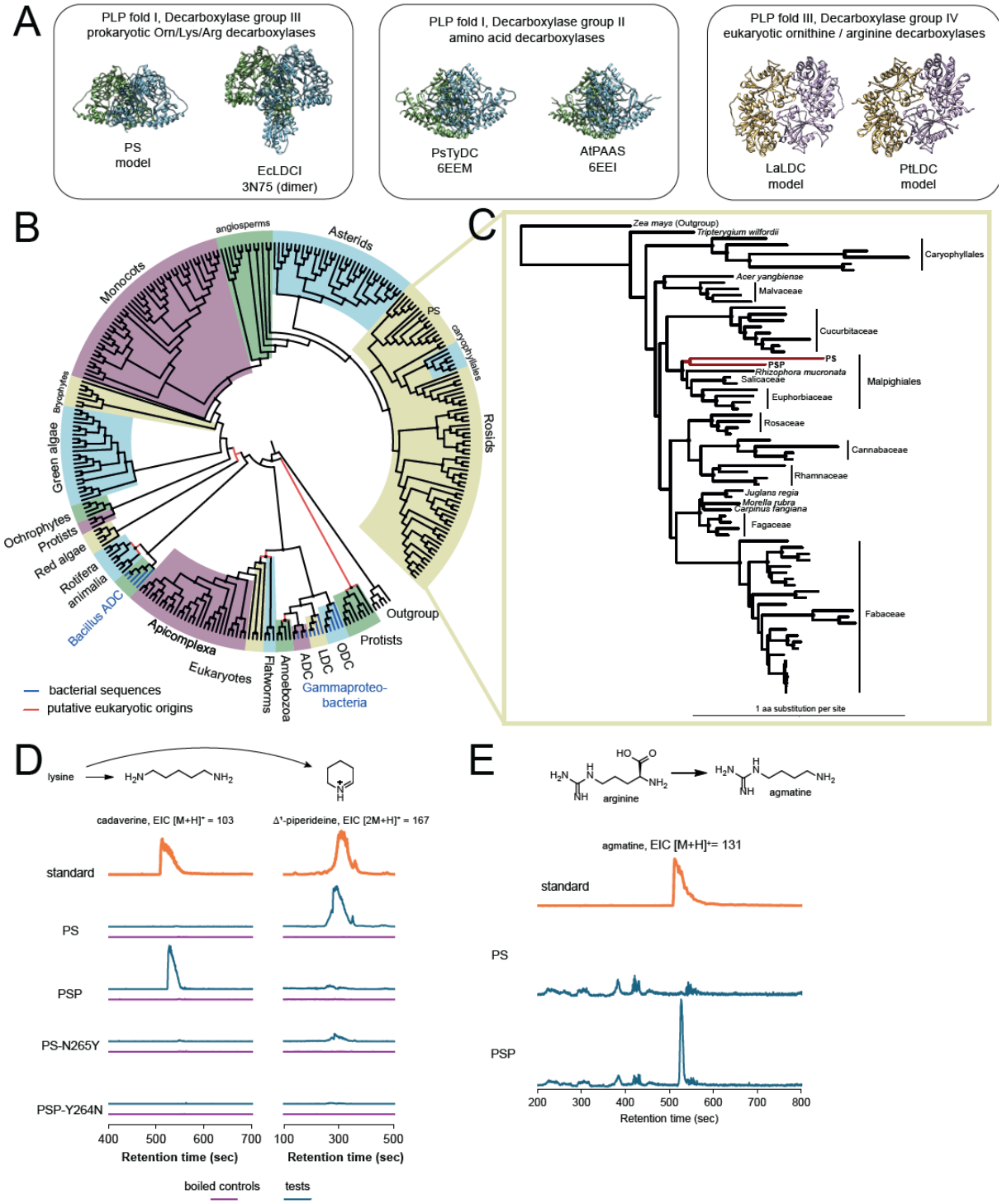

Figure 5. Evolutionary origins of PS. A. X-ray structures or structural models of PLP-dependent decarboxylases. B. Maximum likelihood phylogeny of selected group III decarboxylase protein sequences. Taxonomic clades highlighted by colours. Sequences derived from bacteria are in blue, all other sequences are uncharacterised eukaryotic sequences. Red branches show putative eukaryotic origins. Black dots on nodes show highly supports (SH-aLRT ≥80% and UFboot ≥95%). Sequence names

and branch lengths on **Fig. S6**. C. Focussed rosid phylogeny of selected group III decarboxylase protein sequences. PS and PS paralog highlighted in red. D. Activity of PSP and mutant enzymes with lysine, forming cadaverine or Δ^1-piperideine. E. Decarboxylase activity of PSP with arginine, forming agmatine.

. **Supplementary Figures**

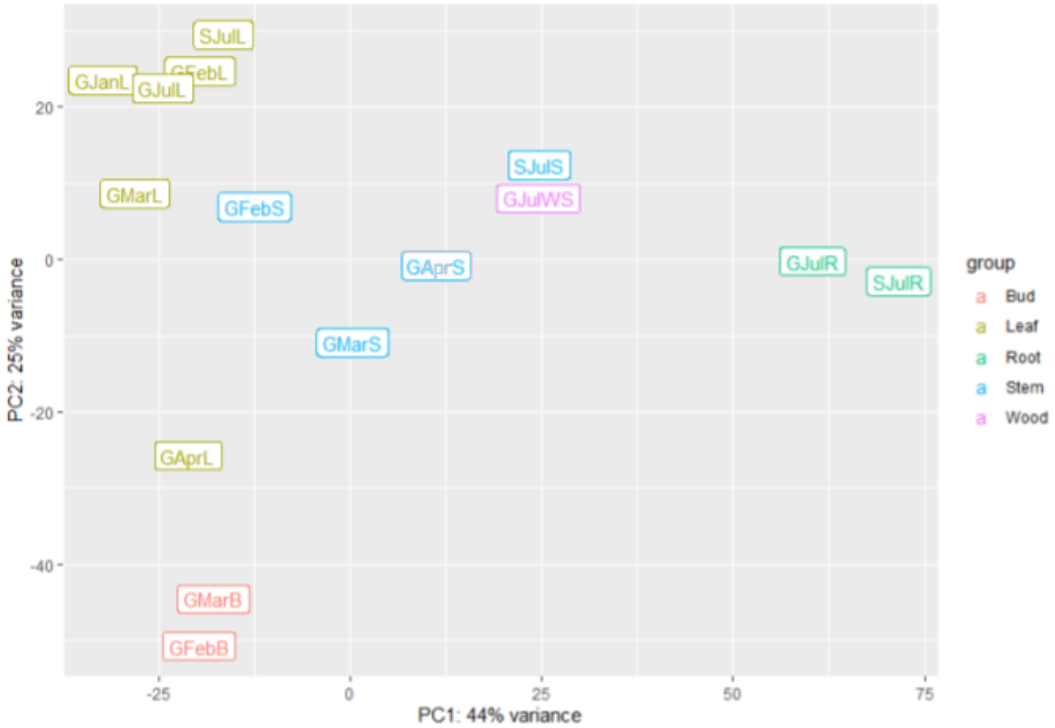

Figure S1. Principle component analysis of RNAseq samples. Principal component analysis (PCA) plot of all 15 samples sequenced. The plot positions samples based on their transcriptional profiles along the first principal component (PC1) on the x-axis, which captures the greatest variance, and the second principal component (PC2) on the y-axis, representing the next greatest variance. Codes for samples in Table S1.

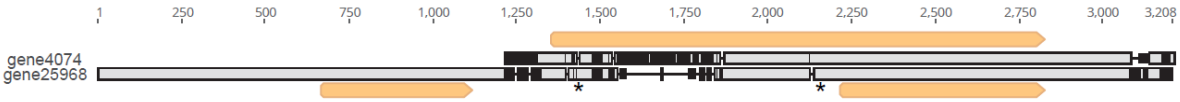

Figure S2. Alignment of two lysine decarboxylase candidates. Nucleotide alignment of genes 4047 (top) and 25968 (bottom). Grey boxed regions are identical, black regions with corresponding lines show gaps. Orange annotations are open reading frames (ATG start, minimum 400 nucleotides). Stars on 25968 show stop codons in frame with long ORF from 4074. The long ORF from gene 4074 was selected as the sequence to be screened.

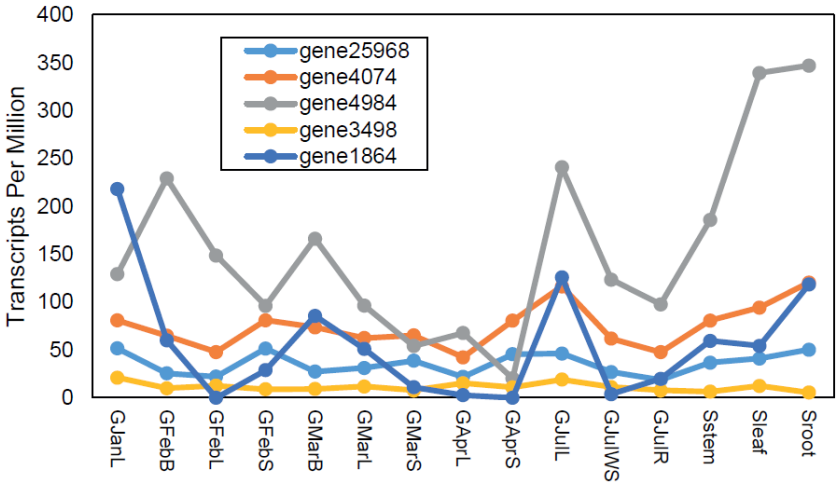

Figure S3. Expression levels of LDC candidate genes. RNAseq determined expression levels across 15 samples. Codes for samples in Table S1.

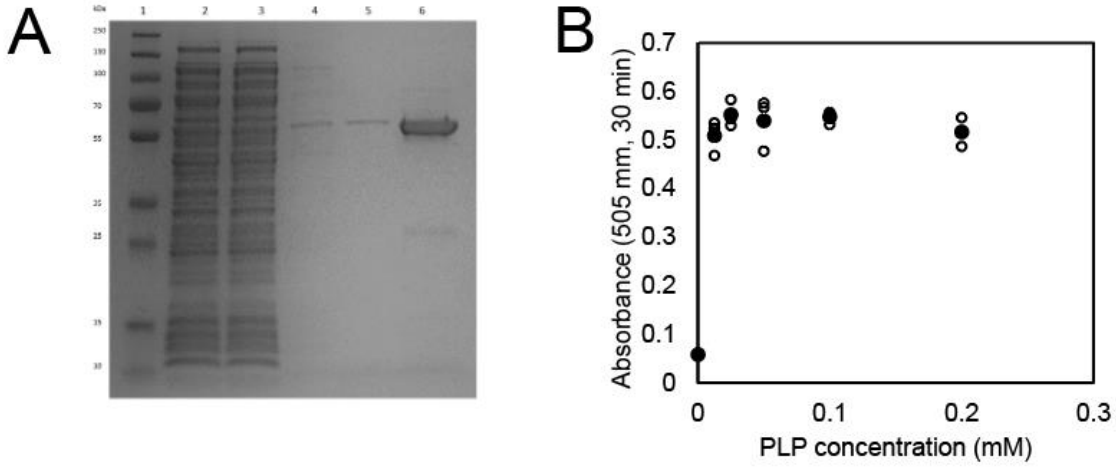

Figure S4. *In vitro* assessment of PS activity. A. SDS-PAGE showing purified Δ74N-PS. Lanes: 1, ladder; 2, clarified lysate; 3, flow-through; 4, wash 20 mM imidazole; 5, wash 40 mM imidazole; 6, 500 mM elution. B. Dependence of H_2O_2 production on PLP concentration, determined by peroxidase coupled assay. Solid circles are means of triplicate measurements. Individual measurements are in hollow circles.

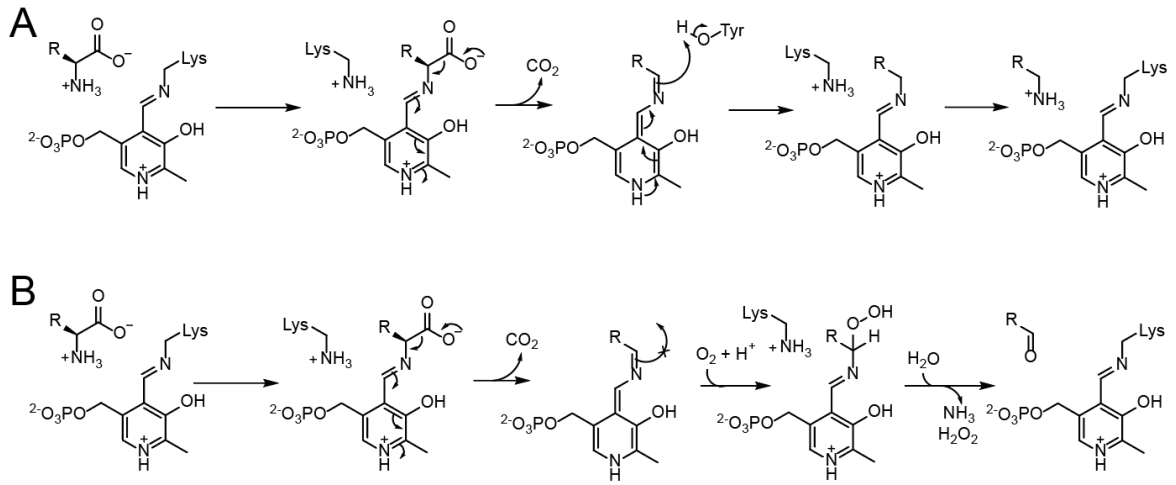

Figure S5. PLP-dependent enzyme mechanisms. A. Typical mechanism of fold-type I PLP-dependent decarboxylase, with mechanistic tyrosine residue. B. Typical mechanism of a fold-type I PLP-dependent oxidative deamination, lacking tyrosine residue. Proposed mechanisms based on Hoffarth *et al* [30].

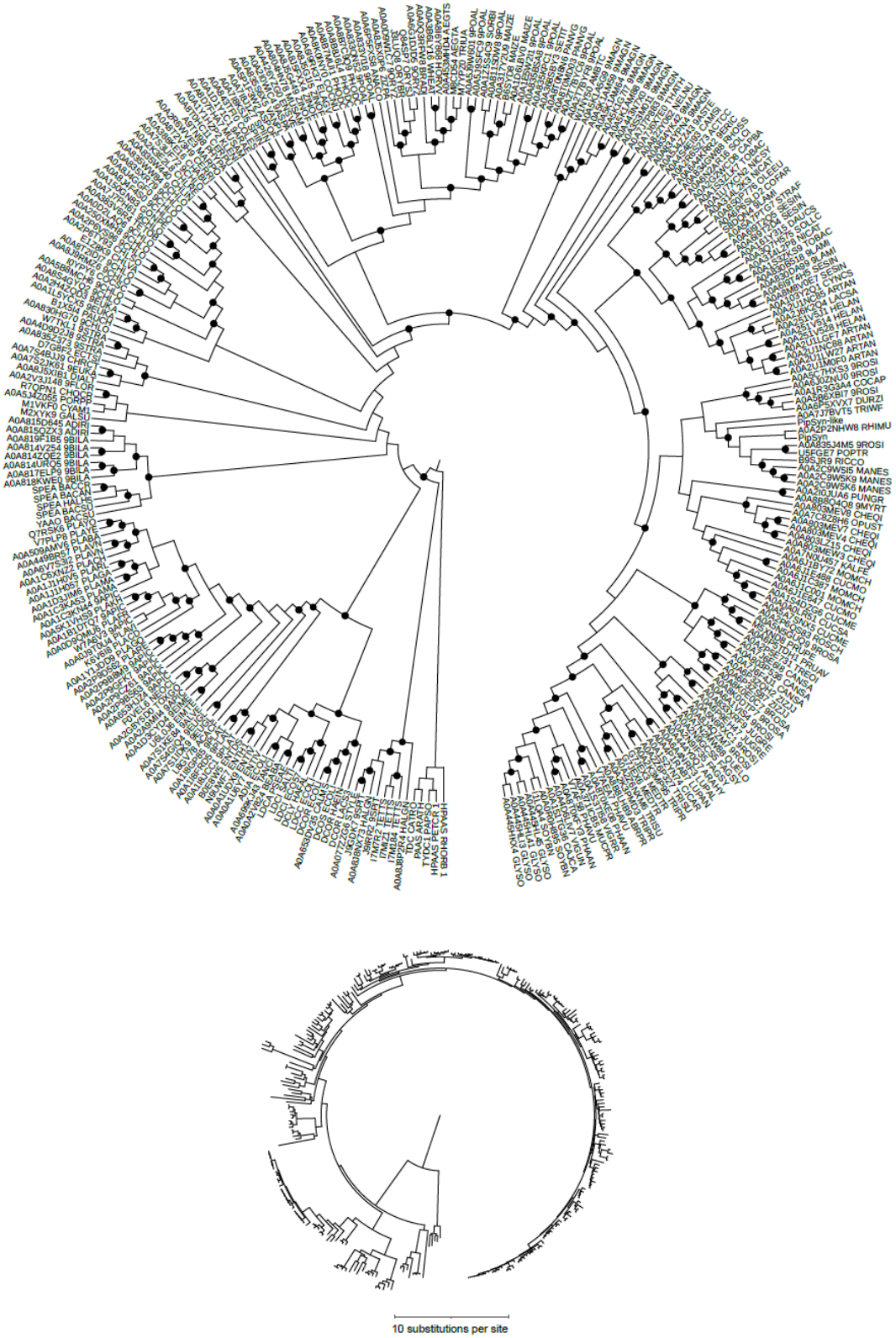

Figure S6. Maximum likelihood phylogeny of group III decarboxylases. Replication of tree in Figure 5B but with Uniprot accession labels (top) and branch lengths (bottom). In top tree, black dots on nodes show highly support values (SH-aLRT ≥80% and UFboot ≥95%).

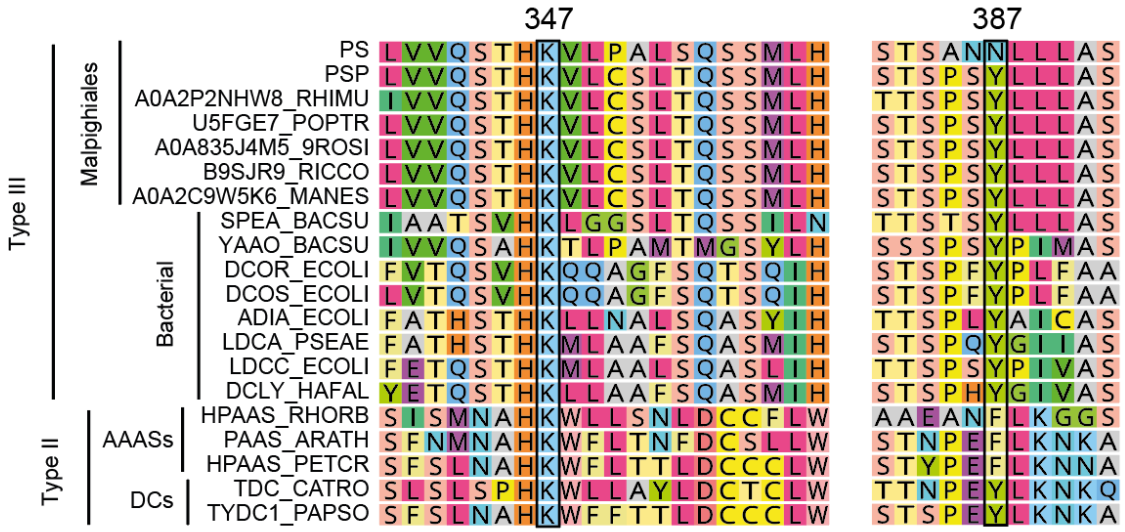

Figure S7. Sequence alignment of PLP-fold type I decarboxylases. Selected aligned regions and sequences showing conserved lysine-347 and mechanistic tyrosine-387. Sequences without tyrosine in that position catalyse oxidative deamination. Numbering of residues determined by PS alignment.

Supplementary Tables

Table S1. RNA Samples. *Flueggea suffruticosa* RNA samples used in the study for *de novo* transcriptome and gene expression analysis. Sequencing available on NCBI (BioProject PRJNA1106657)

Sample Number	Sample code	Plant code	Month	Tissue	Sequencing technology
1	GJanL	G	January	Leaf	Illumina PE150
2	GFebB	G	February	Bud	Illumina PE150
3	GFebL	G	February	Leaf	Illumina PE150
4	GFebS	G	February	Stem	Illumina PE150
5	GMarB	G	March	Bud	Illumina PE150
6	GMarL	G	March	Leaf	Illumina PE150
7	GMarS	G	March	Stem	Illumina PE150
8	GAprL	G	April	Leaf	Illumina PE150
9	GAprS	G	April	Stem	Illumina PE150
10	GJulL	G	July	Leaf	Illumina PE150
11	GJulWS	G	July	Woody stem	Illumina PE150
12	GJulR	G	July	Root	Illumina PE150
13	Sstem	S	July	Stem	Illumina PE150
14	Sleaf	S	July	Leaf	Illumina PE150
15	Sroot	S	July	Root	Illumina PE150
	Pooled samples				ONT MinION
	Pooled samples				ONT PromethION

Table S2. Lysine decarboxylase gene candidates. Candidates selected based on annotation as amine amino acid decarboxylases.

Gene number	Enzyme name	Uniprot Annotation	InterProScan annotation	GenBank accession number
25968		Diaminopimelate decarboxylase	Orn/DAP/Arg decarboxylase	NA
4074		Diaminopimelate decarboxylase	Orn/DAP/Arg decarboxylase	PP748649
4984		Arginine decarboxylase	Orn/DAP/Arg decarboxylase	PP748648
3498	PSP	Arginine decarboxylase	Orn/Lys/Arg decarboxylase	PP748647
1864	PS	Arginine decarboxylase	Orn/Lys/Arg decarboxylase	PP748646

Table S3. Primers. Used to cloned candidates in pHREAC vector. Italics represent homolog overhangs.

Gene Candidate	Direction	Sequence
4074	Forward	*TATATTAAACGTCTCTAAAAATG*GCGGCGACAACGTCTC
4074	Reverse	*AATTTAATGAAACCAGAGCG*TCACAGGCCTTCGAAGAATCG
4984	Forward	*TATATTAAACGTCTCTAAAAATG*CCGGCCCTGGCGTGTTG
4984	Reverse	*AATTTAATGAAACCAGAGCG*TCAAGCACAGCAATAGGACC
1864	Forward	*TATATTAAACGTCTCTAAAAATG*GCTAACAATCAGACTCTCAG
1864	Reverse	*AATTTAATGAAACCAGAGCG*CTACACATCACATATGACTATAG

Online Methods

General

Chemicals and consumables used for molecular biology and biochemistry were obtained from Millipore, Invitrogen, or Merck. Substrates used in enzyme assays were obtained from Sigma-Aldrich. Lysine isotopologs were obtained from CKisotopes (UK distributor for Cambridge Isotope Laboratories). Sanger sequence verification was obtained from Eurofins Genomics or SourceBioscience. Primers were ordered from Integrated DNA technologies. Illumina sequencing was performed by Novogene, ONT sequencing by University of York Bioscience Technology Facility. Sequencing data was analysed using Geneious Prime. Figures were compiled using R-Studio, Microsoft Excel, ChemDraw, Geneious Prime, Chimera, iTOL[43] and Adobe Illustrator.

Plant samples

Flueggea suffruticosa plants (3-5 years old) were obtained from Brighton Plants (Sussex, UK), grown from seed purchased from Chiltern Seeds (Oxford, UK) in January 2014. These seeds originated from a plant in Poland, where it is a common garden ornamental. Prior to sampling, plants were grown in spring-like conditions (20 °C 16 h day, 15 °C 8 h night).

RNA extraction

Samples (i.e. root, stem, old leaves >3 months old, young leaves < 3 months old) were isolated from plants, immediately flash-frozen in liquid nitrogen and ground in liquid nitrogen using a pestle and mortar. Roots were washed thoroughly in water prior to freezing. Frozen ground tissue (100 mg) was extracted using a standard CTAB protocol[44] including a gDNA removal step (Invitrogen™ TURBO DNA-free Kit). The quality of the RNA was assessed using an Agilent 2100 BioAnalyzer, with all samples achieving RNA Integrity Number >8.4.

Illumina short read RNA-sequencing was performed by Novogene (UK) Ltd, enriching for polyA mRNA transcripts, and generating paired end 150 base sequencing reads on an Illumina NovaSeq 6000. Full length cDNA sequencing libraries were prepared using the Oxford Nanopore Technologies (ONT) cDNA PCR barcoding kit (SQK-PCB109), and pooled barcoded libraries were sequenced on ONT MinION and PromethION R9.4.1 flowcells (FLO-MIN106 and FLO-PRO004).

Transcriptome assembly

The ONT reads were base-called using Guppy v5.0.11 and subjected to quality control using PycoQC to ensure the integrity and reliability of the sequencing data[45]. Concurrently, the Illumina reads underwent quality assessment with FastQC, were trimmed of adapters with Cutadapt[46], and ribosomal RNA was removed using BBSplit.

The long-read sequences from all samples were pooled and assembled *de novo* to construct the transcriptome using Rattle[47], a tool optimised for long-read assembly. This initial assembly was then polished with Medaka, employing the ONT reads to correct sequencing errors. To enhance the accuracy of the assembled transcriptome further, three rounds of polishing were conducted using Pilon with the combined Illumina short reads. Post-assembly, the transcripts were filtered through Evigene using the tr2aacds.pl Perl script to remove redundancy and low-quality sequences.

For annotation, the assembled transcripts were first processed with Transdecoder to identify open reading frames (ORFs). Annotation was then performed using BLASTP and BLASTX against the UniProt Swiss-Prot database to identify known protein functions. Protein domains were delineated using InterProScan[28].

Transcriptome quantification

For the quantification of RNA-seq reads, we employed Kallisto, a tool designed for the fast and accurate estimation of transcript abundances through pseudoalignment[48]. Initially, a Kallisto index was generated using our assembled transcriptome as a reference. Reads were then quantified against this index, employing Kallisto's quant command with parameters tailored to our data, including 100 bootstrap samples for uncertainty estimation. The resulting output provided both estimated counts and transcripts per million (TPM) values for each transcript, facilitating downstream analyses such as differential expression.

Transient expression in *Nicotiana benthamiana*

Nicotiana benthamiana plants were grown in F2+S and Calypso insecticide-treated soil in a growth room before and after infiltration (25°C on a 16/8 h day/night cycle). Plants were infiltrated with LBA4404 *Agrobacterium tumefaciens* at 5 weeks old. For preparation of LBA4404 *A. tumefaciens*, chemically competent cells (50 µL) were transformed with plasmid (200 ng) using a heat shock protocol: after mixing cells and plasmids, cells were flash frozen in liquid nitrogen, then defrosted (5 min, 37 °C), and then incubated on ice (30 min). LB media (250 µL) was added, cells were incubated (120 rpm, 2h, 28 °C), and then plated on LB agar (50 µg/mL streptomycin, 50 µg/mL kanamycin). Colonies from plates (after 2–3 days growing at 28 °C) were inoculated into LB media and incubated (50 µg/mL streptomycin, 50 µg/mL kanamycin; 28 °C, 220 rpm, 24 hours). Cells were pelleted (20 min, 4000 xg, RT) and resuspended in infiltration media (10 mM MES, 10 mM $MgCl_2$, 100 µM acetosyringone, OD600 = 0.5) and incubated (RT, 50 rpm, 2 h). Cultures were infiltrated onto the abaxial side of leaves using a 1 mL syringe. One leaf per plant and three plant replicates per plasmid construct were used. For controls we used GFP vector strains (infiltration positive control) and empty vector strain (metabolite negative control). All plants were grown in 16/8 h light/dark, 25 °C, for 5 days before harvest for analysis.

Leaf discs (8 mm diameter) were excised and placed into wells (24 well plate) with buffer (400 µL, 50 mM HEPES, pH 7.5), epidermis facing upwards. Discs were gently pressed to sink to the bottom of the well, and then substrate was added (50 µL, 10 mM lysine). The wells were sealed and placed in a growth chamber for one light cycle (16 h light, 8 h dark, 25 °C). For metabolite extraction, discs were removed from the wells, dried on tissue paper, placed in 2 mL tubes and the tubes frozen in liquid nitrogen. For metabolite isolation, three tungsten carbide beads were added to each tube, and samples were homogenised to a fine powder using a TissueLyser (2x 40 s, 25 Hz) whilst frozen. Solvent was added (200 µL, 80:20 MeOH:H_2O), tubes were vortexed (1 h, RT), and samples centrifuged (10,000 xg, 5 min). Extracts were diluted with MeOH (600 µL), filtered through 0.45 µm PTFE filters and transferred to LC-MS glass vials for subsequent analysis.

Protein expression and purification

For protein expression, *E. coli* Rosetta™(DE3) (Genlantis) was used. Single colonies transformed with plasmids containing genes of interest were used to inoculate overnight cultures with antibiotic selection (2xYT media, 37 °C, 200 rpm). These were diluted with 2xYT with antibiotics (OD600 = 0.1) and grown to OD600 = 0.7 (37 °C, 200 rpm) prior to incubation with IPTG (1 mM) and then incubated overnight (~14 h, 200 rpm, 18 °C). Cell were harvested by centrifugation (3200 xg, 10 min, 4 °C), the supernatant removed, and the pellet resuspend in lysis buffer (10% v/v compared to original culture; 50 mM Tris-HCL, 50 mM glycine, 5% v/v glycerol, 0.5 M NaCl, 20 mM imidazole, pH 8; per 50 mL, 1x EDTA-free protease inhibitor and 10 mg lysozyme) and incubated (30 min, 4 °C). The cells were lysed through a cell disruptor (26 kPsi) and clarified by centrifugation (20 min, 35,000 xg, 4 °C). Purification was achieved through nickel affinity purification using an ÄKTA start FPLC. Clarified lysate was loaded onto a Ni-NTA column (5 mL) and then the column washed with binding buffer (50 mM Tris-HCL, 50 mM glycine, 5% v/v glycerol, 0.5 M NaCl, 40 mM imidazole, pH 8) and the protein eluted (50 mM Tris-HCL, 50 mM glycine, 5% v/v glycerol, 0.5 M NaCl, 500 mM imidazole, pH 8). A protein purification outcome was inspected by SDS-PAGE, and if a pure was protein obtained, samples were buffer exchanged into 50mM HEPES, pH 7.5 using a PD10 column, using a gravity method as per manufacturer instructions. The protein was concentrated by centrifugation (Amicon® Ultra-2 mL Centrifugal Filters, 30 kDa MWCO) prior to addition of glycerol (10% v/v), flash freezing and storage at –70 °C.

Cloning

Initially, genes of interest were identified using the transcriptome assembly and cloned from the plant source. RNA isolated from *Flueggea suffruticosa* (see above) was reverse transcribed to cDNA using Invitrogen™ SuperScript IV kit as per the manufacturer's protocol. The cDNA was immediately used for PCR amplification. Primers were designed that contained an overhang for cloning into vectors (supplementary for primers). PCR was performed using SuperFi™ polymerase

enzyme and amplified genes were isolated using a gel extraction kit. For LaLDC and truncated PS/PSP sequences in *E. coli*, codon-optimised sequences in pET-28a(+) were obtained using gene synthesis (Twist).

Purified pHREAC vector plasmid[49] was digested with BsaI (50 µL reactions; 1 µg DNA, 10 U of BsaI in CutSmart™ Buffer, 37 °C, 1 h) and processed using a PCR clean-up kit (Promega Wizard™). Amplified genes with pHREAC overhangs, deriving either from the cDNA or a plasmid (see above), were inserted into linear pHREAC using In-Fusion HD cloning (with insert:plasmid 2:1). A colony PCR using pHREAC primers (see supp table) was carried out to confirm plasmid transformation and successful cloning. After overnight incubation of transformed *E. coli*, plasmids were miniprepped and sequence verified before transformation into LBA4404 *Agrobacterium tumefaciens*.

In vitro **enzyme Assays**

Reaction components were mixed (100 nM purified protein, 0.1 mM PLP, 50 mM NaCl, 2 mM DTT, 50 mM HEPES pH 7.5, 10 mM substrate, 100 µL final volume). Substrate was added last and the reactions incubated (16 h, 30 °C) prior to quenching with MeCN (400 µL) and LC-MS analysis. For protein controls, proteins were pre-incubated (5 min, 99°C) prior to substrate addition. Reactions were performed in triplicate, with similar outcomes. One representative chromatogram is presented.

LC-MS analysis

Enzyme activity analysis was performed using hydrophilic interaction liquid chromatography (HILIC) as previously described by Nett *et al*.[5]. Analysis was performed using a HPLC instrument Dionex UltiMate 3000, RSLC nano system, with an MS Bruker HCT ultra-ETD II (50-500 m/z collected). The column was an XBridge® BEH Amide column (Waters, 5 µm, 4.6mm x 100 mm). An injection volume of 5 µL was used with an ESI source. Phase A [H_2O 0.125% v/v formic acid, 10 mM ammonium formate] and phase B [95:5 MeCN:Phase A] were used as the mobile phase components. Standards were dissolved in either phase A or B depending on solubility. The chromatography was performed with 0.6 mL/min flow rate and a gradient: 0-4 min, 100% B; 4–24 min, 100–60% B; 24–25 min, 60–100% B; 25–35 min, 100% B. Data was processed in Bruker Compass DataAnalysis Version 4.4.

H_2O_2 Assays

Peroxide formation was detected using phenol and 4-aminoantipyrine (4-AAP) to produce colorimetric readout at 505 nm. Reactions contained: 0.5 mg/mL purified enzyme, PBS pH 8.0, 20 mM lysine, 1 mM DTT, 4 mM phenol, 100 U peroxidase and PLP (0.0125-0.2 mM). Negative control assays were performed without enzyme, and positive controls by the addition of H_2O_2. Spectrophotometric measurements were

taken using a CLARIOstar® Plus UV-Visible spectrophotometer (BMG Labtech) at 505 nm in continuous plate mode. Runs were performed in triplicate.

^{13}C-NMR Assays

Enzyme assays performed as previously described but with ε^{15}N, ε^{13}C-lysine or $^{13}C_6$-lysine. After incubation (16 h, 30 °C), samples were pooled, diluted in 10:90 D_2O:H_2O and place in an NMR tube (S400). The spectrum was measured at 700 MHz using a Bruker NEO spectrometer equipped with a cryoprobe prodigy TCI. 13C spectra used 14,000 scans with a 2s relaxation delay. Data analysis was carried out using MestRe Nova V14.

Synthesis of Δ^1-piperideine

Chemical synthesis of Δ^1-piperideine was conducted at room temperature under an argon atmosphere. Δ^1-piperideine was synthesised using a variation of a previously described protocol[50]. Piperidine (5.00 g, 5.90 mL, 58.7 mmol) was added dropwise to a stirred solution of *N*-chlorosuccinimide (8.34 g, 62.5 mmol) in Et_2O (60 mL). The resulting mixture was stirred for 2 h, and the solids were removed by filtration. The filtrate was washed with water (2 x 35 mL), dried (with Na_2SO_4) and evaporated under reduced pressure to give an oily residue. A solution of NaOMe in MeOH, freshly prepared by carefully adding sodium metal portionwise (1.53 g, 66.7 mmol) to MeOH (35 mL) until the sodium had been fully consumed, was added to the oily residue at RT. The resulting solution was stirred and heated at reflux for 45 min. After cooling to room temperature, water was added until all the solids had dissolved. Et_2O was then added, the layers were separated, and the aqueous layer was extracted with Et_2O. The combined organic layers were evaporated under reduced pressure until a sticky residue remained. Et_2O (100 mL) was added to the residue, and the solution was dried (with $MgSO_4$) to yield Δ^1-piperideine. The NMR data obtained matched those previously described[50].

Protein structural analysis

Structural models of enzymes were constructed using AlphaFold2 and AlphaFold2-multimer on ColabFold[51]. PLP cofactors were added with AlphaFill. The best scoring model was selected for display. For dimers of PS, the unstructured N-terminal sequence was removed prior to calculation. The structural models, along with X-ray structures were depicted using Chimera (UCSF). For EcLDCI (PDB: 3N75) selected subunits of the homo 10-mer were depicted to enable visual comparison.

Phylogenetic analysis

For phylogenetic analysis of the group III decarboxylase proteins, sequences of proteins containing the Orn/Lys/Arg decarboxylase, major domain were obtained from InterPro (IPR000310). Of bacterial sequences, only those which were Swiss-Prot “Reviewed” were kept. All eukaryotic sequences were selected, along with PS/PSP

from *F. suffruticosa*, and the group II outgroup. Then duplicate and obsolete sequences were removed, as were sequences with <400 residues and those without Pfam PF01276 OKR_DC_1 annotation. After alignment with MAFFT[52], sequences were further curated by removing those missing the PLP binding lysine and the conserved glycine (570 on PS), selecting a single sequence from those with >95% sequence identity with others, and removing sequences with large alignment gaps with respect to PS residues 98-580. A maximum likelihood tree was then inferred using W-IQ-TREE[53] with ModelFinder[54], ultrafast bootstraps (UFBoot2, X1000)[55], and SH-aLRT supports (X1000)[56]. For the rosid phylogeny, selected sequences were obtained, realigned with MAFFT, then columns with >95% gaps were removed prior to tree inference with W-IQ-TREE. Trees were depicted using iTOL[43].